Mon. Not. R. Astron. Soc. **358,** 291–304 (2005) doi:10.1111/j.1365-2966.2005.08806.x

Photoionizing feedback in star cluster formation

J. E. Dale,[1⋆] I. A. Bonnell,[2] C. J. Clarke[3] and M. R. Bate[4]

[1]*Department of Physics and Astronomy, University of Leicester, University Road, Leicester LE1 7RH*
[2]*School of Physics and Astronomy, University of St Andrews, St Andrews, Fife KY19 9AJ*
[3]*Institute of Astronomy, Madingley Road, Cambridge CB3 0HA*
[4]*School of Physics, University of Exeter, Stocker Road, Exeter EX4 4QL*

Accepted 2005 January 7. Received 2005 January 6; in original form 2004 July 1

ABSTRACT

We present the first ever hydrodynamic calculations of star cluster formation that incorporate the effect of feedback from ionizing radiation. In our simulations, the ionizing source forms in the cluster core at the intersection of several dense filaments of inflowing gas. We show that these filaments collimate ionized outflows and suggest such an environmental origin for at least some observed outflows in regions of massive star formation. Our simulations show both positive feedback (i.e. promotion of star formation in neutral gas compressed by expanding H II regions) and negative feedback (i.e. suppression of the accretion flow in to the central regions). We show that the volume filling factor of ionized gas is very different in our simulations from the result from the case where the central source interacted with an azimuthally smoothed gas density distribution. As expected, gas density is the key parameter in determining whether or not clusters are unbound by photoionizing radiation. Nevertheless, we find – on account of the acceleration of a small fraction of the gas to high velocities in the outflows – that the deposition in the gas of an energy that exceeds the binding energy of the cluster is *not* a sufficient criterion for unbinding the bulk of the cluster mass.

Key words: stars: formation – H II regions.

1 INTRODUCTION

It has long been recognized that massive stars deposit considerable mechanical and thermal energy into the interstellar medium (ISM) by a variety of processes. On galactic scales, the main feedback agent is supernova explosions (e.g. McKee & Ostriker 1977; Dekel & Silk 1986); however, the relatively long time lapse before supernovae explode – compared with the dynamical time-scale in star-forming regions – ensures that supernovae are ineffective in regulating star formation in the close vicinity of the progenitor. At the opposite extreme of length-scales, radiation pressure on dust operates in the region (a few hundred au from a typical OB star) where dust is close to its sublimation temperature. This form of feedback is thus mainly instrumental in controlling the formation of the OB star itself (Wolfire & Cassinelli 1986, 1987; Yorke & Sonnhalter 2002; Edgar & Clarke 2003, 2004).

On intermediate scales (∼pc), stellar winds and photoionization are likely to play the primary role in regulating the formation of star *clusters* (e.g. Tenorio-Tagle et al. 1986, 1999, 2003). On one hand, the star formation rate may be enhanced by the fragmentation of shells of dense gas swept up by winds/expanding H II regions (e.g. Elmegreen 1998; Elmegreen, Palouš & Ehlerová 2002; Whitworth & Francis 2002), but the acceleration and expulsion of gas from the neighbourhood of the OB star also ultimately limits the fraction of a molecular cloud core that can be turned into stars. This latter effect has important implications for the formation of bound star clusters, as, by simple energetic arguments, a cluster cannot remain bound if it rapidly loses more than 50 per cent of its original mass (Hills 1980; Lada, Margulis & Dearborn 1984). See also Goodwin (1997), Adams (2000), Geyer & Burkert (2001) and Boily & Kroupa (2003) for more sophisticated analyses of this problem. Although the majority of stars form in clusters (Clarke, Bonnell & Hillenbrand 2000), most of these clusters are already unbound at an age of $\sim 10^7$ yr (Battinelli & Capuzzo-Dolcetta 1991). It is likely, at least in clusters that contain more than a few hundred members – and are thus populous enough to contain an OB star – that such feedback effects are decisive in unbinding nascent clusters.

Feedback is also likely to be the main factor that regulates the Galactic star formation rate (SFR). It has long been recognized that the observed SFR in the Milky Way of a few $M_\odot$ yr^{-1} is only a few per cent of the value that would result if all the giant molecular clouds (GMCs) in the Galaxy were turning into stars on their internal dynamical time-scales (Zuckerman & Evans 1974). Although one solution is that star formation in GMCs is quasistatic – i.e. is regulated, perhaps by magnetic fields, so that it occurs on a time-scale considerably longer than the dynamical timescale (e.g McKee 1989) – recent reappraisals of the characteristic lifetime of GMCs suggest

⋆E-mail: Jim.Dale@astro.le.ac.uk

© 2005 RAS

Downloaded from https://academic.oup.com/mnras/article/358/1/291/1036608 by U.S. Department of Justice user on 16 August 2022

that star formation is rapid but also swiftly terminated (Elmegreen 2000; Hartmann 2003). In this latter model, only a few per cent of the mass of a cloud ends up being incorporated into stars prior to its dispersal. Simple estimates, based on homogeneous molecular clouds, suggest that dispersal either by photoionization (Whitworth 1979; Franco & Garcia-Segura 1996) or by OB stellar winds (Clarke & Oey 2002) would give rise to a star formation efficiency of this order.

To date, however, numerical feedback studies have been limited to the case of highly idealized cloud structures, i.e. smooth density profiles with spherical or axial symmetry (Yorke et al. 1989; Franco, Tenorio-Tagle & Bodenheimer 1990; Garcia-Segura & Franco 1996). Axisymmetric calculations demonstrate how feedback operates preferentially in directions of steeply declining density and suggest that the net effect of feedback in clouds that are realistically inhomogeneous may be very different from that in smoothed density fields. Although some consideration has been given to the propagation of radiation in inhomogeneous clouds (e.g. Hobson & Padman 1993; Hobson & Scheuer 1993; Witt & Gordon 1996; Röllig, Hegmann & Kegel 2002; Hegmann & Kegel 2003), particularly with regard to explaining spatial variations in the abundances of photosensitive species, such calculations have not hitherto been combined with hydrodynamical star formation simulations. The reason for this is that radiation transport is most readily handled by Eulerian schemes, where it is relatively straightforward to perform integrals along optical paths. Such schemes are, however, challenged by the large density contrasts that develop in realistic star formation simulations, although adaptive mesh refinement (AMR) methods are becoming an increasingly powerful tool in this regard (Klein et al. 2003; Tassis et al. 2003).

In this paper, we present pilot calculations of photoionization feedback in smoothed particle hydrodynamics (SPH) simulations of star cluster formation in realistically inhomogeneous clouds. [These simulations do not currently incorporate feedback from stellar winds, which may turn out to be a reasonable omission on the time-scale of these simulations ($\sim 10^5$ yr), as there is some suggestion that the youngest OB stars have anomalously weak winds; Martins et al. (2004)]. Our calculations employ an algorithm for the inclusion of photoionization in SPH. Briefly, this method locates the ionization front at every hydrodynamical time-step and adjusts the temperature of the gas behind the front accordingly. The ionization front is located by comparing the flux of ionizing photons emitted in the direction of a given particle with the integrated recombination rate between the source and that particle. In this (Strömgren volume) technique, the integrated recombination rate is calculated as though the density structure between the particle and the source represented the radial variation of a spherically symmetric density distribution. Evidently, this approach depends on the validity of the on-the-spot approximation (i.e. on the assumption that diffuse ionizing photons resulting from recombinations to the ground state are absorbed locally). Our method also implicitly assumes that the ionization structure adjusts instantaneously to any changes in the gas distribution due to, for example, outflows. This assumption is valid provided that the time-scale on which the gas distribution evolves is longer than the local recombination time-scale, which is always the case in the simulations presented here. We note the generic similarity between the present algorithm and that proposed by Kessel-Deynet & Burkert (2000), inasmuch as both use the on the spot approximation and utilize the SPH neighbour lists to construct integrated recombination rates in an efficient manner; however, whereas Kessel-Deynet and Burkert evaluated the evolution of the ionization fraction of each particle using time-dependent ionization equations, our method – by locating a Strömgren volume – assigns to each particle a wholly ionized or wholly neutral state at each time-step. The method turns out to be simpler and more robust than that of Kessel-Deynet and Burkert and is justified by the sharpness of the ionization fronts in the high-density environments we consider. A detailed description of the code and the results of one-dimensional tests will be published in a subsequent paper.

In reality, although the boundary of the H II region under such conditions is very sharp, the boundary between hot and cold gas is likely to be less so, as the non-ionizing photons from the radiation source would produce a photodissociated region (PDR) outside the H II region, where the temperature might reach 1000 K (Diaz-Miller, Franco & Shore 1998). The overall effect of this phenomenon is not easy to predict as, on one hand, the smaller pressure gradient across the ionization front will retard the expansion of the H II region, but the additional thermal energy deposited over a greater volume of the cluster may increase the total mass involved in outflows. We do not treat PDRs in this work, but the combined action of H II regions and PDRs would make an interesting subject of further study.

We also do not take into account the likely presence of dust in our H II regions. Wood & Churchwell (1989) found evidence of dust in *all* of the ultracompact H II regions (UCHIIRs) in their survey and estimated that the dust was absorbing between 50 and 90 per cent of the photon flux emitted by the source in each case. Considerable theoretical work has been performed on the effect of dust on H II region evolution. Diaz-Miller et al. (1998) suggest that there exists an additional initial phase of H II region expansion in which the dust content of the ionized gas is either destroyed or expelled by the radiation field of the star. Detailed numerical calculations by Arthur et al. (2004) suggest that Wood & Churchwell's (1989) estimates of the fraction of ionizing photons absorbed by dust were too large in most cases. In any case, reduction of the photon flux of a source by 90 per cent results in a reduction in the size of the equilibrium Strömgren sphere by only $\sim$50 per cent. We therefore expect that inclusion of dust in our calculations would have little effect on our results, although it would probably slightly increase the time-scale for expansion of our H II regions.

For these pilot simulations, we plumb our photoionization algorithm into the simulations of the formation of a massive star cluster by Bonnell & Bate (2002). Specifically, we introduce ionizing radiation from a single source in the cluster core, $\sim$1 initial free-fall time after the initiation of the collapse. For our present purposes, the important feature of the protocluster at the time that photoionization switches on is that the gas distribution is highly inhomogeneous, with the cluster core lying at the intersection of several high-density filaments that channel an accretion flow into the core. Although the Bonnell & Bate calculation is scale free (i.e. can be scaled to any system of isothermal gas containing the same number of initial Jeans masses in gas and the same number of point masses initially), the introduction of feedback necessarily introduces an absolute mass scale to the calculation. Our approach here has been to apply two different scalings to the Bonnell & Bate calculations, so as to explore the efficiency of feedback in relatively high- and low-density environments.

In Section 2 we describe briefly the calculations performed by Bonnell & Bate (2002) and the way in which we used these calculations to form the initial conditions for our study of photoionizing feedback. In Section 3, we describe a high- and a low-resolution calculation of a protocluster in which the gas densities were high (10^5–10^9 cm^{-3}). In Section 4, we describe a single low-resolution calculation of a system with much lower gas densities (10^3–10^6 cm^{-3}). In Section 5 we compare the two suites of simulations

Downloaded from https://academic.oup.com/mnras/article/358/1/291/1036608 by U.S. Department of Justice user on 16 August 2022

with simple one-dimensional calculations to assess the effect on the efficiency of feedback of the complex internal structure of our protoclusters and of the gravitational field of the ionizing sources within them. In Section 6 we go on to draw conclusions.

2 INITIAL CONDITIONS

Feedback in all its forms is dominated by massive stars, so the study of the effects of feedback requires an understanding of the formation of high-mass stars. Although the formation of low-mass stars is moderately well-understood, the formation of high-mass stars is well known to be problematic. In particular, there has been considerable debate as to whether or not stars more massive than $\sim 10\,\mathrm{M}_\odot$ can form by conventional accretion, due to the effect of radiation pressure on dust (Wolfire & Cassinelli 1986, 1987; Yorke & Sonnhalter 2002; Edgar & Clarke 2003, 2004).

Bonnell, Bate & Zinnecker (1998) proposed an alternative scenario for massive star formation, namely that massive stars form by the collision and merger of lower-mass stars. Bonnell & Bate (2002) explored this scenario by performing numerical calculations at two resolutions. The high-resolution calculation was run on the UK Astrophysical Fluids Facility (UKAFF) facility at Leicester University, while the low-resolution run was conducted on a SUN workstation. Their initial conditions were a cluster containing $1000\,M_\mathrm{J}$ of isothermal gas and 1000 low-mass stellar 'seeds' whose total mass corresponded to 10 per cent of the gas mass and $\approx$9 per cent of the total mass of the system. They arranged the gas and stars in a spherically symmetric Gaussian density distribution with zero velocity initially. Mergers between two stars were permitted if they approached each other within a distance of 10^{-5} times the initial cluster radius.

In both their calculations, Bonnell & Bate found that accretion increased the stellar density in the cluster core enough to allow stellar collisions to occur, contributing in both simulations to the formation of a central object sufficiently massive to have a strong photoionizing flux. In this paper, we take the end results (after approximately a free-fall time) of their simulations as the initial conditions of our own calculations. At this point, $\sim$7 per cent of the gas had accreted on to the stars, increasing the mean stellar mass by $\sim$70 per cent. In addition, the mean stellar density increased by a factor of 10 and the maximum stellar density (defined by the minimum volume required to contain 10 stars) rose by a factor of $\simeq 10^5$. This proved to be sufficient to allow 19 stellar mergers and contributed to the formation of a very massive star in the cluster core. We emphasize that our choice of this system as a testbed for introducing photoionization feedback is motivated largely by the fact that it shares several features with observed young clusters. In particular, we wish to explore conditions in which the ionizing star is located near the cluster centre and in which the gas distribution is highly anisotropic.

We conducted three calculations, designated UH-1, SH-1 and SL-1. In all of our calculations, we dispensed with stars and gas at large radii and rescaled Bonnell & Bate's calculations by adjusting the length unit in the code to allow us to study two different regimes of behaviour. In UH-1 and SH-1, we study at two different resolutions virtually identical protoclusters where the gas densities are ($\sim 10^4$–$10^8\,\mathrm{cm}^{-3}$). UH-1 is based on Bonnell & Bate's UKAFF run and SH-1 on their SUN run. In both of these calculations, we also rescaled the ambient temperature of the neutral gas to retain the absolute value of the Jeans mass. This resulted in ambient temperatures of $\sim$1.4 K, which are obviously unrealistically low, but we point out that varying the value of the ambient temperature by a factor of a few will have a negligible effect on the dynamical evolution of these calculations, as the behaviour of the protoclusters will be dominated by the thermal pressure of the hot ionized gas and the ram pressure of the accretion flows, both of which are several orders of magnitude greater than the ambient thermal pressure even before rescaling. These calculations are described together in Section 3.

In SL-1, also based on Bonnell & Bate's SUN run, we simulate a protocluster with significantly lower gas densities ($\sim 10^3$–$10^6\,\mathrm{cm}^{-3}$). We elected not to rescale the ambient temperature in this calculation, instead leaving it at 10 K. This calculation is described in Section 4. In all of the calculations, we used our Strömgren volume technique to define the H II region at each hydrodynamic time-step, heating the gas within to 10 000 K. The properties of our three model clusters are given in Table 1.

Table 1. Parameters of our runs. All gas densities quoted are atomic hydrogen number densities.

	UH-1 run	SH-1 run	SL-1 run
Particle number	5×10^5	5×10^4	5×10^4
Total mass ($\mathrm{M}_\odot$)	742	745	745
Initial stellar mass ($\mathrm{M}_\odot$)	225	223	223
Initial gas mass ($\mathrm{M}_\odot$)	517	522	522
Initial radius (pc)	1.4	1.4	2.8
Initial Jeans mass ($\mathrm{M}_\odot$)	0.8	0.8	40.5
Core gas density (cm^{-3})	$\sim 10^9$	$\sim 10^8$	$\sim 10^6$
Mean gas density (cm^{-3})	$\sim 10^4$	$\sim 10^4$	$\sim 10^3$
Free-fall time (yr)	1×10^6	1×10^6	2×10^6
Source luminosity (s^{-1})	6×10^{49}	6×10^{49}	2×10^{49}

3 SIMULATIONS OF HIGH-DENSITY INITIAL CONDITIONS

We describe the UH-1 and SH-1 runs together in this section as they are essentially simulations of the same protocluster differing only in their numerical resolution. In common with Bonnell & Bate (2002), we conducted our high-resolution UH-1 simulation on the SGI Origin 3800 of the UK Astrophysical Fluids Facility and the corresponding low-resolution one on a SUN workstation. The initial conditions for the UH-1 and SH-1 simulations, given in Table 1, were quantitatively almost identical. The ionizing source in these calculations has an initial mass of $\sim 30\,\mathrm{M}_\odot$. We regard it as a point source of ionizing photons and assign to it an ionizing flux of $6 \times 10^{49}\ \mathrm{s}^{-1}$. This is a rather generous output even for such an O-star ($2 \times 10^{49}\ \mathrm{s}^{-1}$ would be more realistic), but is justified, as the ionizing star in these simulations grows considerably in mass (to a few$\times 100\,\mathrm{M}_\odot$) through further accretion (see Diaz-Miller et al. (1998) for a table of O-star ionizing luminosities). We note that this luminosity is close to the classical Eddington luminosity of the source, but accretion continues along the gaseous filaments, as the inhomogeneous structure of the gas increases the effective Eddington luminosity of the source (see Shaviv 2001, for a discussion of super-Eddington accretion in inhomogeneous environments).

3.1 The UH-1 run

In Fig. 1, we plot the initial radial density profile of the UH-1 protocluster. There is clearly an enormous range of gas densities in the system. The profile approximately follows a power law with slope $\alpha \approx -2$, but there is evidently a great deal of substructure superposed on this general configuration. This can be seen in detail in Fig. 2, which shows a column-density map of the protocluster (the ionizing source is at the centre of the image).

Downloaded from https://academic.oup.com/mnras/article/358/1/291/1036608 by U.S. Department of Justice user on 16 August 2022

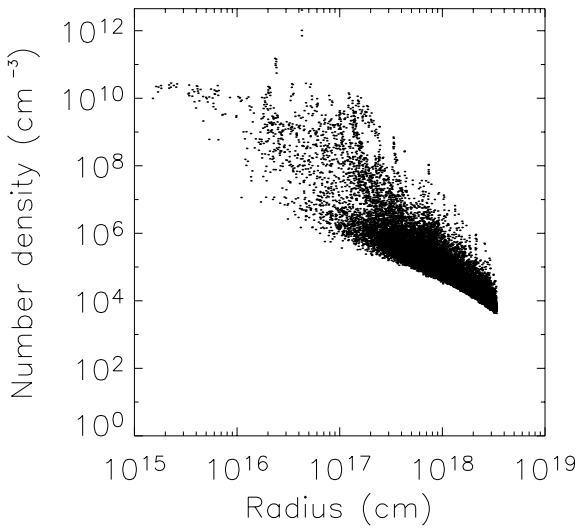

Figure 1. Initial radial density profile of the UH-1 calculation. Only every tenth particle has been plotted.

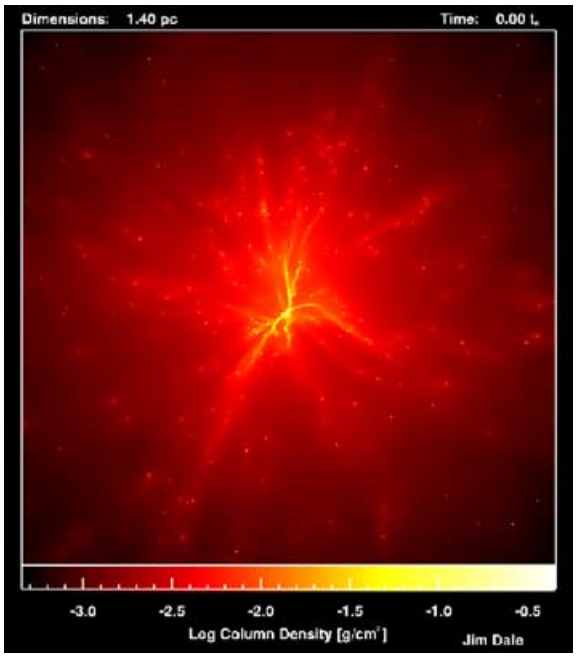

Figure 2. Column density map of the inner 1.4×1.4 pc^2 of the initial conditions for our UH-1 calculation as viewed along the z-axis.

It can be seen that the initially smooth gas in Bonnell & Bate's original calculation has developed a complex filamentary structure, which approximately radiates outwards from the core. The distribution of residual gas closely follows that of the stars, with stars being preferentially located inside gaseous filaments. These structures are due to gravitational instabilities in the gas, which amplify pre-existing shot noise in the stellar seed distribution. One of the aims of this study is to see what effect this structure has on the efficacy of feedback.

The gas is distributed highly anisotropically with respect to the O-star at the centre of the protocluster. Fig. 3 shows a θ, ϕ column density map of the cloud as seen from the ionizing source. One expects that this structure will result in the distance to which ionizing

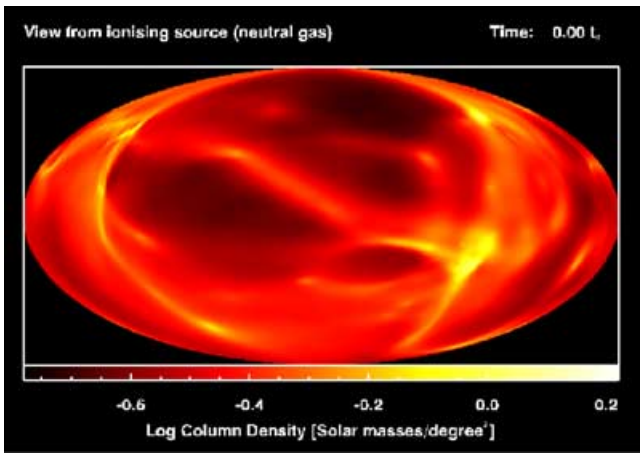

Figure 3. θ, ϕ column density map of the gas distribution in the UH-1 cluster at the beginning of the simulation as seen from the ionizing source. Only material within 0.2 pc has been included in this map in order to emphasize the anisotropic conditions encountered by the radiation field of the source.

radiation can penetrate the protocluster to be similarly anisotropic and our simulations demonstrate that this is true.

We found that ionizing radiation is able to escape from the immediate vicinity of the massive star in only a few directions, forming several outflows and corresponding elongated H II regions. The radiation and thus the outflows are loosely collimated by the dense gas near the star. By restricting the directions in which radiation can escape from the source, a small mass of gas distributed very close to the ionizing source is able to dominate the evolution of the ionized region and thus to control its effect on the rest of the cloud. Bonnell & Bate suggested such collimation as a possible explanation for the poorly collimated outflows observed around young massive stars. This work lends considerable support to this proposal. However, we note here that this collimation may be due, in part, to noise in the particle distribution close to the source, as a single particle at a small radius is potentially able to shield a large number of particles further out in the cloud. This importance of this effect could be studied by splitting gas particles close to the source into $\sim$10 (for example) smaller, lower-mass particles, but the presence of particles of very different masses in the same region of space can give unphysical results in SPH. We have not investigated this issue.

The end result of our calculation is shown in Fig. 4 at which point the ionizing source has been radiating for $\sim 1.7 \times 10^5$ yr, $\sim$17 per cent of the global free-fall time of the cluster.

3.1.1 Outflows

The outflow structure is evidently very complex. Watching an animation of the simulation allows six or seven individual radial flows to be identified. These outflows are visible as the dark regions in Fig. 5, a second θ, ϕ plot of the gas column density seen from the source, generated at the same epoch as Fig. 4. The disposition of the outflows is interesting in that they are all confined to the left-hand half of the cloud. Hence, the left-hand hemisphere of the cloud has a radically different structure by the end of the calculation, whereas the right-hand hemisphere is almost untouched.

The outflows are weakly collimated. Their opening angles can be estimated by eye from Fig. 5 and are $\sim 10^\circ$–20°. The ionized gas in the outflows expands azimuthally and radially, sweeping up neutral material and generating numerous fresh filamentary structures,

Downloaded from https://academic.oup.com/mnras/article/358/1/291/1036608 by U.S. Department of Justice user on 16 August 2022

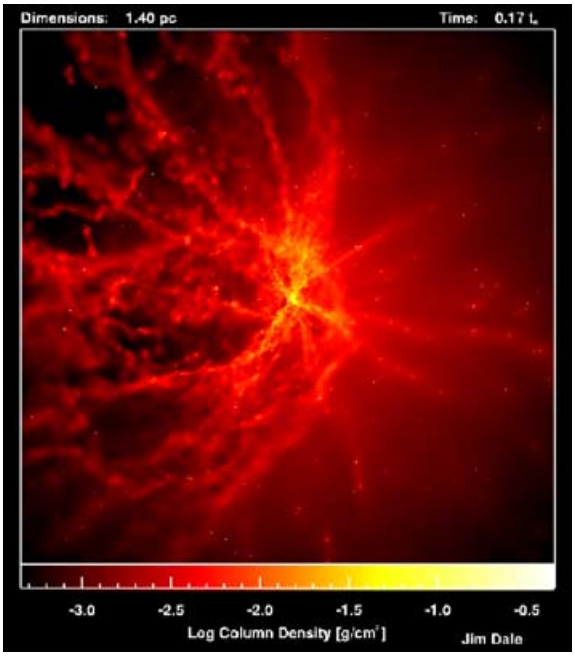

Figure 4. Column density map showing the end result of the UH-1 calculation after $0.17\,t_{ff}$, as viewed along the z-axis. Note the asymmetric distribution of the outflows.

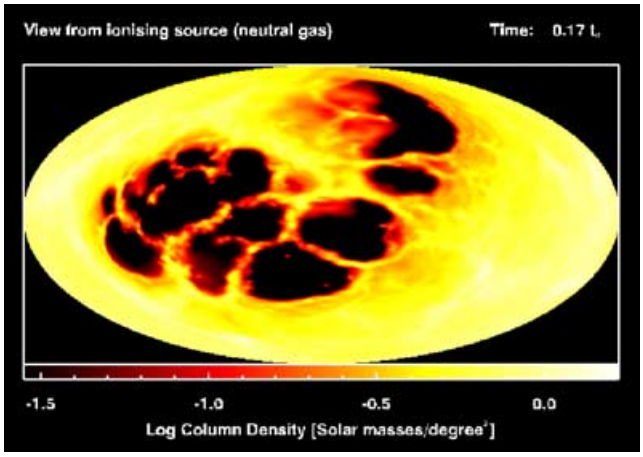

Figure 5. A θ, ϕ column density map of the neutral gas distribution as seen from the source in the UH-1 calculation at $t = 0.17 t_{ff}$. All neutral gas has been included in this map.

particularly where neutral gas is caught between two expanding bubbles. These filaments are also visible in Fig. 5 as the narrow bright features within the dark areas of the plot. The filamentary structures subsequently fragment into strings of clumps whose densities increase with time, as they are immersed in hot ionized gas and are therefore under strong compression. At the point where we were forced to stop the simulation, the entire left-hand hemisphere of the protocluster is a chaotic assembly of chains of isolated clumps and filaments still in the process of subfragmentation. The right-hand hemisphere of the cloud remains largely untouched because of shielding by very dense material just to the right of the ionizing source. It can be seen in the animation that the source is beginning to clear away this material and it is likely that the protocluster would become more homogeneous if it were possible to continue

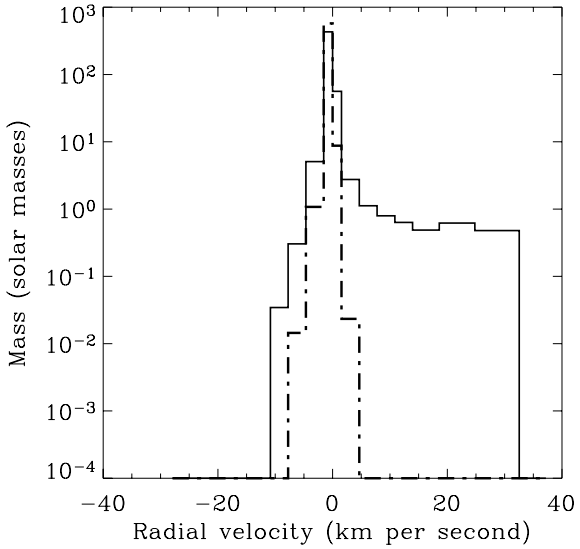

Figure 6. Histograms showing the initial distribution of velocities with mass (dotted lines) and the final distribution including the outflows driven by the thermal pressure of the ionized gas in the UH-1 calculation, as described in the text (solid lines).

the simulation. However, we were forced to terminate the simulation prematurely because numerous particles acquired time-steps which were prohibitively short, slowing the calculation dramatically. This is due to the development of strong density enhancements owing to the increased fragmentation.

We compare the mass entrained in the outflows and the momentum this mass carries with outflows observed in real star-forming regions. In Fig. 6, we plot histograms showing the masses of gas involved in inflows and outflows at the beginning and at the end of the simulation. Initially, most of the gas in the system is infalling at speeds of 5 km s^{-1} or less. The outflows are clearly visible in the overlaid later plot as material with high positive radial velocities. The total mass involved in the outflows is $\sim 30\,M_\odot$, ~ 7 per cent of the total gas mass. Only approximately one-third of the gas involved in the outflows is ionized, the remainder being swept-up neutral gas. The mean rate at which the outflows are removing mass from the cluster core is $\approx 2 \times 10^{-4}\,M_\odot\ yr^{-1}$. The total outflow momentum is $\approx 10^3\,M_\odot$ km s^{-1}, in good agreement with observed values as tabulated by Churchwell (1997) for stars in the spectral range B0–O4.

Although this agreement with the parameters of observed outflows is encouraging, we note here that the outflows in our simulations, which are driven by anisotropic heating, are not in general bipolar in nature, as their number and symmetry is determined purely by details of the initial gas structure near the radiation source. At first sight, this would appear to disfavour such a mechanism as outflow sources from young massive stars are usually described as being bipolar (e.g. Beuther et al. 2002; Kumar, Bachiller & Davis 2002). However, as noted by Shepherd, Churchwell & Wilner (1997), this designation can be misleading, as outflow lobes may not be symmetric and some outflows appear to be monopolar. The outflows described here clearly cannot be compared with the highly collimated sources recently discovered in pre-UCHIIRs (Beuther et al. 2002; Davis et al. 2004), but they may be compatible with some of the less collimated objects described by Shepherd et al. (1997). It is currently unclear what fraction of observed outflows could be explained by the mechanism we discuss here, and what fraction

Downloaded from https://academic.oup.com/mnras/article/358/1/291/1036608 by U.S. Department of Justice user on 16 August 2022

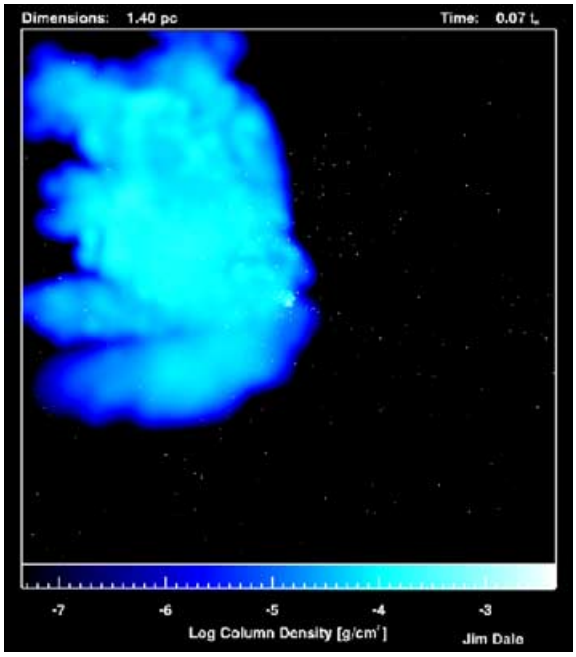

Figure 7. Column density map of the ionized gas in the UH-1 simulation $0.07\,t_{ff}$ after source ignition revealing the unusual shape of the H II region.

require the conventional scenario of bipolar flows emanating from an accretion disc.

3.1.2 H II regions

The structure and behaviour of the ionized gas in this simulation is unusual for two reasons. First, the H II region possesses a multilobed structure due to the beaming effects mentioned in the preceding paragraphs. An example is shown in Fig. 7, showing clearly that the H II region(s) generated in these calculations bear little resemblance to the classical picture of the Strömgren sphere. Although unusual, the H II region depicted in Fig. 7 is in appearance not unlike some of the 'cometary' ultracompact H II regions described in Wood and Churchwell's seminal paper on the subject (Wood & Churchwell 1989), in particular G29.96-0.02 (shown on p. 863 of Wood & Churchwell 1989) and G43.89-0.78 (shown on p. 867).

The second unusual property of our H II regions is their variability. In the early stages of the simulation, the H II regions are observed to 'flicker' on short time-scales (a few hundred to a few thousand years), frequently disappearing completely, only to regrow a short time later. This can be seen in Fig. 8 where we plot the fraction of the gas of the protocluster that is ionized as a function of time. Although the general tendency is for the ionization fraction to increase, it exhibits numerous sharp rises and falls, particularly in the early stages of the calculation.

Fig. 8 implies, particularly in the early stages of the simulation, that the H II region contains small numbers of SPH particles, sometimes below the canonical resolution limit of $\sim$50, corresponding to a particle and its neighbours. We conducted convergence tests in a uniform spherically symmetric model cloud to determine what effect such apparent underresolution might have on the expansion of the H II regions in our simulations. We found that we were able to reproduce the well-known Spitzer solution for the expansion of a spherical H II region in a uniform cloud (Spitzer 1978) even when the H II region initially contained as few as three(!) SPH particles.

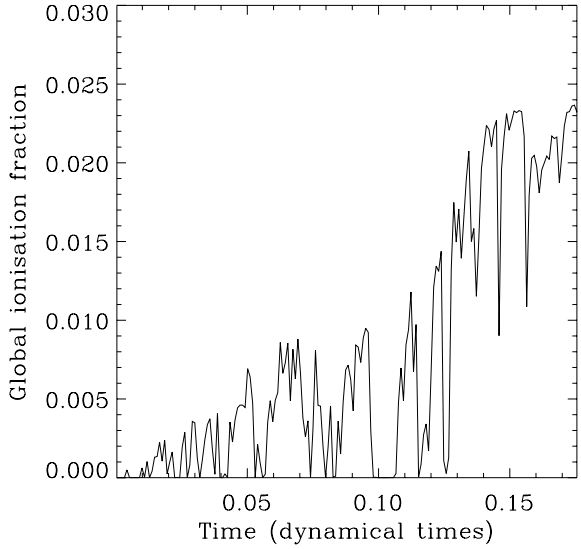

Figure 8. A plot of the UH-1 global ionization fraction of the protocluster as a function of time, revealing the flickering process described in the text. The dynamical time of the system is 10^6 yr.

We concluded from this that the resolution requirements pertinent to modelling the expansion of H II regions are rather less stringent than those relevant to other physical processes, although clearly the accuracy with which the detailed geometry of H II regions can be modelled is dependent on the available resolution.

The cause of the flickering behaviour is the rapid and non-uniform accretion taking place in the core of the protocluster, mostly along the dense filaments. Although, in the simulations, this effect is partly shaped by finite resolution near the source (i.e. the effect of individual SPH particles), it is more generally the case that small fluctuations in the amount of neutral matter near the source can have a profound effect on the propagation of ionizing radiation to large radii. At early times, the interplay of the expanding H II regions and the accretion flows results in the source region being intermittently inundated by inflowing neutral gas on a characteristic time-scale similar to the free-fall time-scale in the cluster core. As this time-scale is long compared with the recombination time-scale anywhere in the cluster, the H II regions are able to respond by switching on and off on this time-scale (see Fig. 8). However, after $\sim 10^5$ yr, a quasi-steady flow pattern is set up, in which the neutral flow never completely swamps the core region and the mass of ionized gas thereafter grows steadily with time.

Once the H II region has reached its stable phase, it is able to have a dramatic effect on the structure of the gas in the protocluster, as ionized gas is able to permeate a significant fraction of the volume of the cluster (although the ionization fraction in this simulation was never more than 3 per cent). We observed the emergence of a great deal of novel structure, but we were not able to follow the evolution of the protocluster long enough to study the gross dynamical effects of photoionizing feedback. We therefore turn to the low-resolution SH-1 calculation, which was able to run for significantly longer.

3.2 The SH-1 run

The SH-1 calculation was started from similar (although not identical) initial conditions to those of the UKAFF run and was able to continue for considerably longer, allowing us to study the long-term dynamical impact of the H II region on our protocluster and to

Downloaded from https://academic.oup.com/mnras/article/358/1/291/1036608 by U.S. Department of Justice user on 16 August 2022

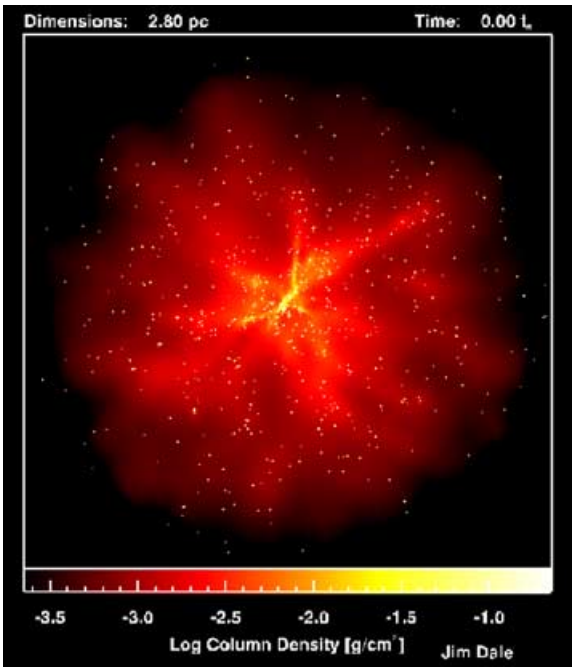

Figure 9. Column density map of the initial conditions for our SH-1 calculation as viewed along the z-axis.

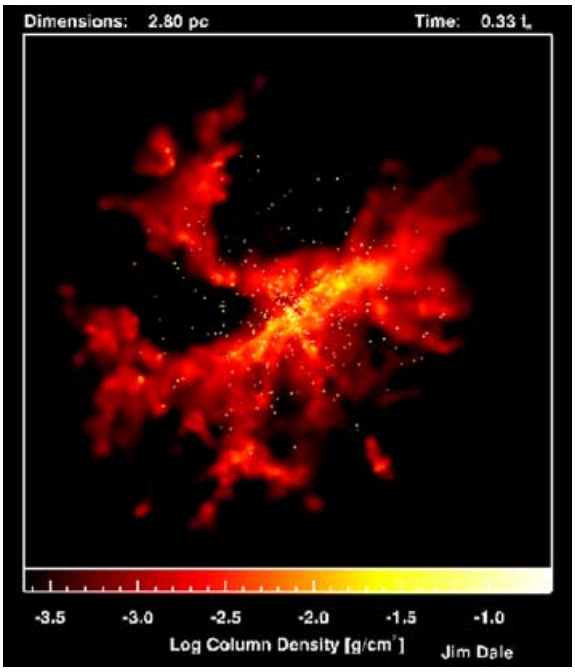

Figure 10. Column density map of the end result our SH-1 calculation after $0.33\,t_{ff}$, as viewed along the z-axis.

determine the effect of the fragmentation process observed in the high-resolution run on the star formation within the cloud. The initial conditions for these calculations are shown in Fig. 9. They are clearly qualitatively similar to those of the high-resolution run, as can be seen by comparing Figs 2 and 9.

The evolution of the low-resolution simulation was similar to the UKAFF calculation, as shown in Fig. 10. We again observed several weakly collimated outflows driving bubbles of ionized gas into the ambient neutral gas of the protocluster, generating filamentary and bead-like structures as they went. We also observed the phenomenon of H II-region flickering, depicted in Fig. 11, again dying away as the ionizing source was able to expel some of the dense gas from its immediate vicinity and deflect the accretion flows away from the core. However, in this case, we are more interested in the later evolution of the system.

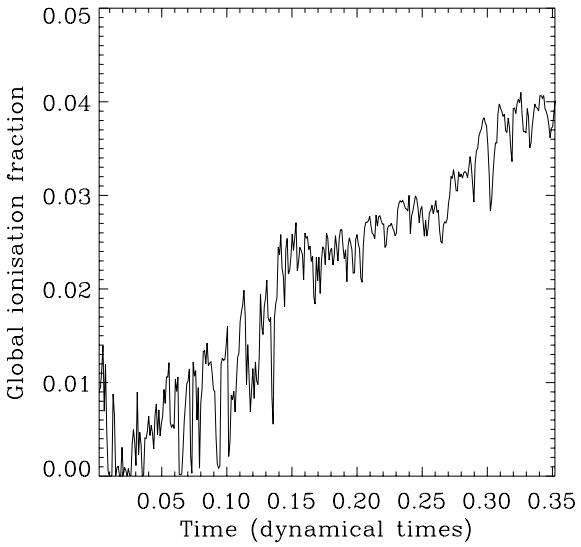

Figure 11. A plot of the global ionization fraction as a function of time for our SH-1 calculation. As in the UH-1 run, we observe that the H II region initially flickers rapidly before settling down to a stable expansion phase. The dynamical time of the system is 10^6 yr.

3.2.1 Accretion, energy uptake and cluster survival

The most obvious question to ask is whether or not the radiation from our massive star is able to prevent the cluster from becoming permanently gravitationally bound. At the beginning of our simulations, the cluster is bound, but the ratio of gas mass to stellar mass is ∼2.5:1, so rapid expulsion of significant quantities of gas could unbind the cluster. As accretion is still in progress in the core of the cluster, this ratio is clearly approaching 1:1 as time progresses. If the ratio of gas mass to stellar mass reaches 1:1 while the system is still globally bound, the cluster, or at least its stellar content, will remain bound regardless of what happens to the remaining gas. The question of whether or not feedback can unbind the cluster therefore reduces to seeing if the accretion flows can be stopped before this occurs. In Fig. 12, we show how the total masses of the stellar and gaseous components of the protocluster evolve with time in the SH-1 calculation. We compare the SH-1 calculation with another one identical except that the ionizing source was left switched off. In both plots, all the gas and all the stars in the clusters are included whether still bound to the cluster or not, so the change in the masses of the two components is due purely to accretion.

The global accretion rates in the two simulations are given by the gradients of the lines in Fig. 12. The accretion rate in the case with feedback active is lower than in the run without feedback but accretion is never halted because the thermal pressure of the ionized gas is considerably less than the ram pressure of the accretion flows. The stellar and gas masses reach equality at a later time with feedback active but examination of the energies of the stellar and gaseous components of the cluster revealed that all the stars and ∼83 per

Downloaded from https://academic.oup.com/mnras/article/358/1/291/1036608 by U.S. Department of Justice user on 16 August 2022

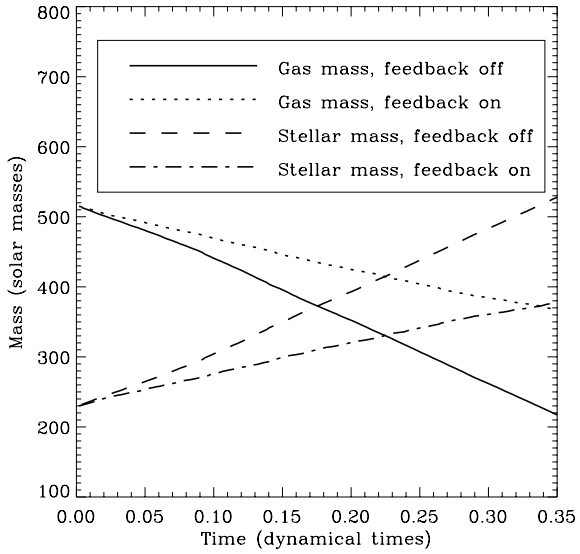

Figure 12. Comparison of the evolution of the masses of the SH-1 stellar and gaseous components of the cluster in runs with feedback active and inactive. The dynamical time of the system is 10^6 yr.

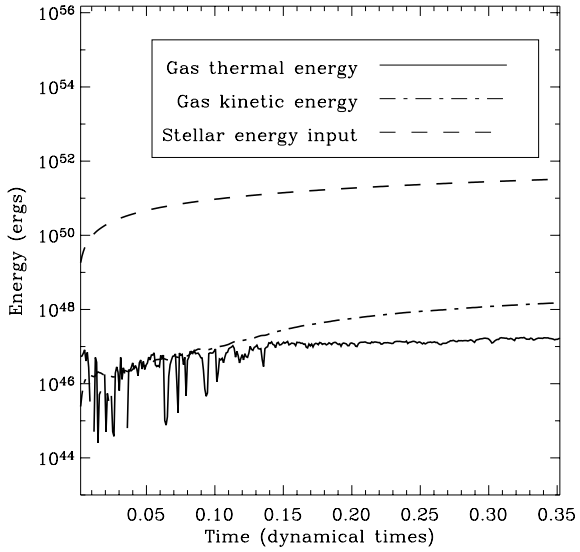

Figure 13. Comparison of the stellar energy input with the gas thermal and kinetic energies in the SH-1 calculation. The dynamical time of the system is 10^6 yr.

cent of the gas are still bound at this point in time, so photoionizing feedback has failed to unbind the cluster.

We now compare the stellar energy input with the thermal and kinetic energies of the gas to see how efficiently the energy emitted by the ionizing source is being taken up by the system and we compare the total energy uptake with the gravitational self-energy of the cluster. The gravitational potential energy of an object of mass M and radius r is given approximately by

$$E_{\rm grav} \simeq \frac{GM^2}{r}. \quad (1)$$

Our protocluster has a total mass of 740 $M_\odot$ and a radius of 4.2×10^{18} cm, giving $E_{\rm grav} \simeq 3 \times 10^{46}$ erg. In Fig. 13, we plot the gas thermal and kinetic energies against time along with the energy input by the star since its ignition [taking this to be the energy contained

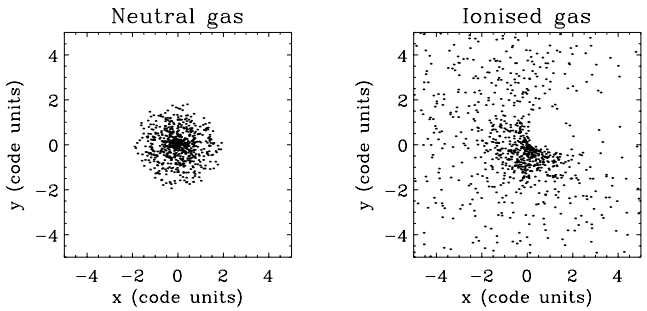

Figure 14. *xy*-plots of the positions of neutral and ionized gas particles in the SH-1 run, revealing that the hot ionized gas is able to effectively escape the protocluster.

in 6×10^{49} 13.6 eV photons $s^{-1} \times$(time since ignition)]. Two things are immediately apparent form Fig. 13: first, the photoionization process in this cluster is extremely inefficient, with <0.1 per cent of the energy injected by the star being retained. We have assumed that all recombinations of ions with electrons that initially deposit the electron in an atomic energy state other than the ground-state result in the emission of a photon or a series of photons to which the gas is optically thin. Such recombinations therefore constitute an energy sink. In addition, at the end of the calculation, ∼20 per cent of the ionizing flux is escaping from the cloud directly, through holes in the gas distribution.

Secondly, despite the inefficient coupling, the star apparently *has* deposited enough energy into the gas to unbind the cluster as a whole.

This leads to the obvious question of why the cluster does not become globally unbound. The answer is simply that, although sufficient energy has been absorbed by the cluster gas to exceed the total gravitational binding energy of the cluster, this energy is distributed throughout a small proportion (∼17 per cent) of the gas. As can be seen in Fig. 14, the ionized gas is escaping from the cluster, entraining some neutral gas with it, and carrying thermal and kinetic energy away, so this energy has little effect on the cloud as a whole. Although the energetic material becomes unbound, the remainder, constituting over 83 per cent of the gaseous component of the cluster, is still firmly bound within the gravitational potential well of the cluster.

Our neglect of the likely existence of a PDR outside the H II region in these calculations clearly affects the energetics of our cluster. The presence of a PDR would result in the thermal energy of the cluster gas being higher and may also increase the kinetic energy of the gas by involving a larger fraction of it in outflows. However, the results presented in this section suggest that *where* in the cluster thermal energy is deposited is at least as important as the bare quantity of energy. The expansion of the H II region in this protocluster was controlled by the dense material and accretion flows near the radiation source and it is likely that the PDR would be similarly constrained. We think it unlikely that modelling the PDR would substantially alter our conclusions.

3.2.2 Star formation

In none of our simulations was the mass resolution good enough to follow the star formation process in detail, but we can draw qualitative conclusions concerning the effect of feedback from the evolution of the mean Jeans mass of the cluster, depicted in Fig. 15, where we have again made a comparison with the control simulation without feedback. In both cases, the mean Jeans mass was estimated

Downloaded from https://academic.oup.com/mnras/article/358/1/291/1036608 by U.S. Department of Justice user on 16 August 2022

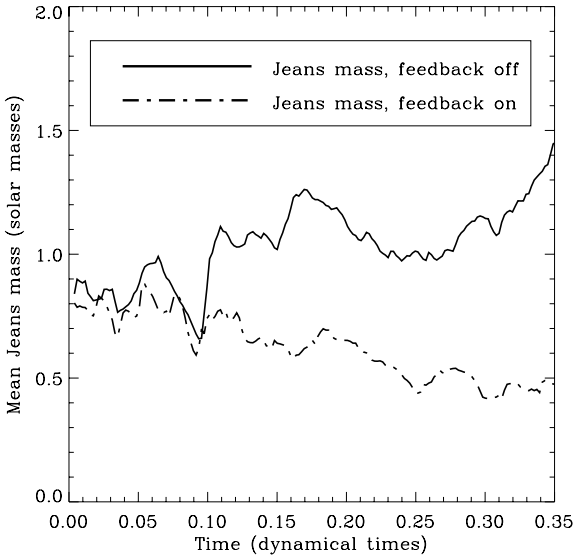

Figure 15. Evolution of the mean Jeans mass within the SH-1 cluster. The dynamical time of the system is 10^6 yr.

using the mean density of the *neutral* component of the cluster gas only, comprising not less than 95 per cent of the total gas mass of the feedback run (and 100 per cent of that in the control run), taking the neutral gas in both runs to have the initial ambient temperature. The evolution of the mean Jeans mass in the two systems is initially similar, but becomes very different after $\sim 0.1\, t_{ff}$. Although both plots exhibit rapid fluctuations, the general trend in the control run is for the Jeans mass to increase, whereas in the feedback run, the Jeans mass decreases. The former result is counterintuitive: as the system is collapsing unimpeded, one might expect the mean gas density to rise and the Jeans mass to fall (given that the temperature is constant). However, because of the rapid accretion taking place in the control simulation and because high-density gas in the cluster core is accreted more rapidly than low-density gas further out in the cluster, the mean gas density in this calculation actually *decreases* overall.

In the feedback calculation, the accretion rate is considerably lower, as shown in Fig. 12 and it is in the core that the accretion rate is most affected. In addition, the spread of hot ionized gas throughout much of the volume of the cluster results in the compression and fragmentation of much of the remaining neutral gas in the system – this process can be clearly seen in Fig. 4 by comparing the highly fragmented left-hand-side of the cloud with the almost-untouched right-hand side. The net result of these effects is that the mean gas density in the feedback calculation *increases*, driving the Jeans mass down (non-monotonically) from its initial value of from $\approx 0.8\,\mathrm{M}_\odot$ to $\approx 0.4\,\mathrm{M}_\odot$. Although the mass resolution of the calculation ($\sim 0.5\,\mathrm{M}_\odot$) is not sufficient to follow the fragmentation/star formation process (and indeed only a few new stars were observed to form during the simulation), we can infer from this plot that the overall effect of the ionizing source is to decrease the mean Jeans mass of the protocluster and thus to promote fragmentation. We cannot, however, make any statements regarding how many new stars will actually form.

4 SIMULATIONS OF LOW-DENSITY INITIAL CONDITIONS

In the previous section, we studied a cluster in which the feedback effects of the massive stars were strongly constrained by the physical

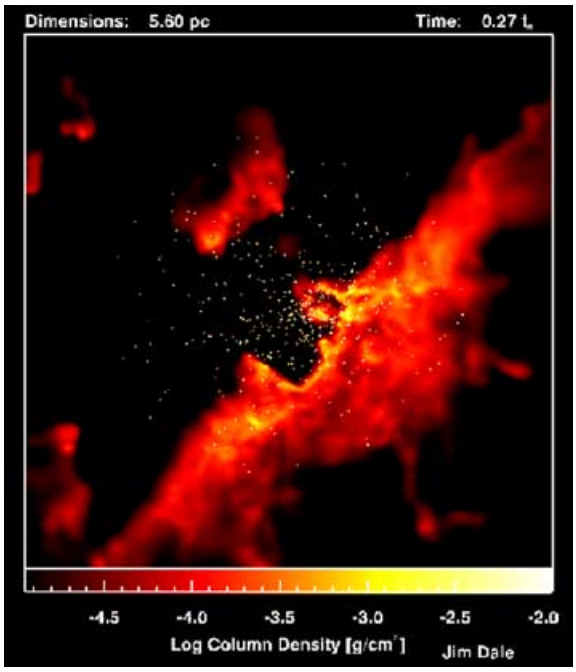

Figure 16. Column density map of the end result of the SL-1 run after $0.27\, t_{ff}$, as viewed along the z-axis.

structure and dynamical properties of the gaseous component of the system. We now consider a protocluster in which the gas density is approximately an order of magnitude lower and on which we therefore expect feedback to have a greater impact.

4.1 The SL-1 run

In our SL-1 simulation, we study a cluster in which the gas density is considerably lower (as we have increased the physical size of the cluster), in an attempt to give feedback an opportunity to have a greater influence on the dynamical evolution of the protocluster. The ionizing source in this simulation had an initial mass of $\sim 30\,\mathrm{M}_\odot$, rising to $\sim 60\,\mathrm{M}_\odot$ by the end of the run. It was assigned an ionizing photon flux of 2×10^{49} s^{-1}.

4.1.1 Accretion, energy uptake and cluster survival

The evolution of this simulation is markedly different from that of either of the foregoing calculations. Fig. 16 shows a column-density map of the end result. Although superficially similar to Fig. 10, careful inspection shows that photoionization has been more successful in expelling gas from the core of the protocluster in the low-density simulation. As can be seen by close examination of Figs 10 and 16, there is a higher degree of segregation between the stars and the gas in the SL-1 simulation and this has been achieved on a shorter time-scale than in the SH-1 calculation. Because of the lower gas densities in the SL-1 system, the radiation source is able to partially ionize and thus disrupt the radial accretion flows. Fig. 17 shows a plot of the global ionization fraction in the SL-1 run. Although the flickering phenomenon observed in the UH-1 and SH-1 calculations does occur in this run, it dies away much more rapidly, allowing the ionization fraction to rise more monotonically and to attain higher values, although only by a factor of a few. The disruption of the accretion flows has the natural consequence that the global accretion

Downloaded from https://academic.oup.com/mnras/article/358/1/291/1036608 by U.S. Department of Justice user on 16 August 2022

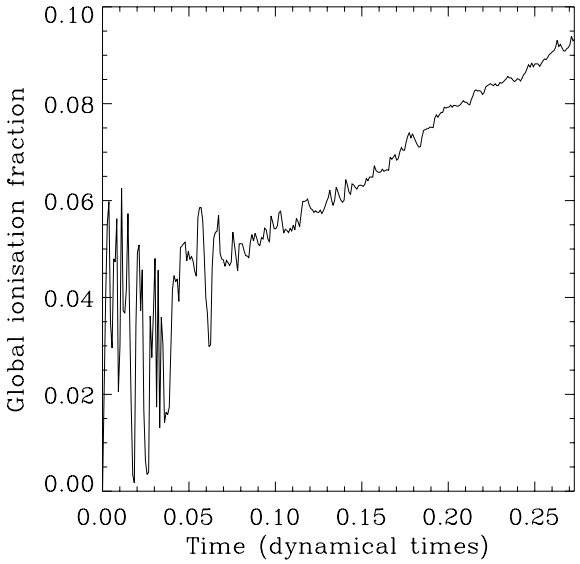

Figure 17. Evolution of the global ionization fraction in the SL-1 calculation. The dynamical time of the system is 2×10^6 yr.

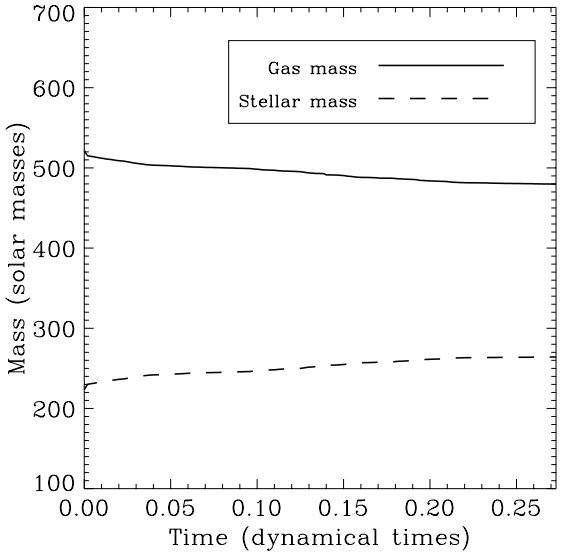

Figure 18. The accretion behaviour of the SL-1 calculation. The dynamical time of the system is 2×10^6 yr.

rate in the SL-1 run is lower. Fig. 18 shows that feedback quickly brings accretion to an almost complete halt, leaving the stellar:gas mass ratio little changed from its initial value.

As shown in Fig. 19, the energy transfer in this calculation is significantly more efficient than in the SH-1 simulation, despite the fact that ∼70 per cent of the ionizing flux is escaping from the system at the end of the run. In addition, the gravitational binding energy of this system is significantly lower ($\sim 10^{46}$ erg), so the SL-1 protocluster is 'easier' to unbind. This is reflected in the dynamical end-states of the calculations. In the SH-1 calculation, the fraction of gas still gravitationally bound at the 'point of no return' where the total stellar mass comes to exceed the total gas mass was 83 per cent and accretion was still in progress, so the SH-1 protocluster was almost certain to remain globally bound. In contrast in the SL-1 protocluster, accretion is almost halted by feedback and the

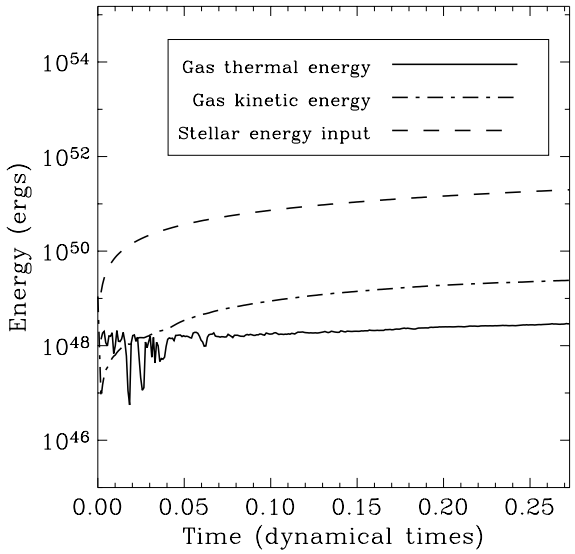

Figure 19. Comparison of the stellar energy input with the gas thermal and kinetic energies in the SL-1 run. The dynamical time of the system is 2×10^6 yr.

bound gas fraction drops to less than 65 per cent by the end of the simulation, ∼0.27 free-fall times after source ignition. 5 per cent of the stars are also unbound at this point. We expect the fraction of unbound stars to rise as more gas is expelled from the system, but it is not possible to say on the basis of this calculation whether any of the stellar population of the cluster will remain bound or not.

As in the SH-1 simulation, the energetics of this system have been modelled ignoring the likely existence of a PDR surrounding the H II region, which would result in the deposition of a larger quantity of thermal energy in the gas and over a larger volume. It is probable that modelling this effect would lead the SL-1 protocluster to become unbound faster but, again, we do not feel that our conclusions would be significantly different.

4.1.2 Star formation

We qualitatively assess the impact of feedback on star formation in the SL-1 cluster by examining the evolution of the mean Jeans mass, again estimated using the mean density of the *neutral* gas of the protocluster content only and taking its temperature to be the initial ambient temperature. The result is shown in Fig. 20. After $\sim 0.05\, t_{ff}$, the mean Jeans mass increases sharply by ∼50 per cent. This is due to destruction of dense filaments of neutral gas near the radiation source by expanding ionized gas. Although this process continues throughout the calculation, it is counterbalanced by the compression of neutral gas further out in the protocluster as it is swept up by the growing H II region. Comparison of the SH-1 and SL-1 calculations reveals that feedback has two competing effects on the gas in protoclusters. Which effect dominates is determined by the gas density of the system. Feedback can decrease the gas density in the cluster core by destroying the structure there, but this effect was not observed in the high-density calculations because this material was simply too dense. Conversely, feedback can raise the gas density in the outer reaches of the cluster by sweeping up neutral gas and generating new structure. This latter effect dominated in UH-1 and SH-1 calculations, driving the global mean gas density up and the mean Jeans mass down. In the SL-1 calculation, the two effects roughly cancel each other for most of the run and the mean Jeans mass changes little. However, after $0.2\, t_{ff}$, disruption of the dense

Downloaded from https://academic.oup.com/mnras/article/358/1/291/1036608 by U.S. Department of Justice user on 16 August 2022

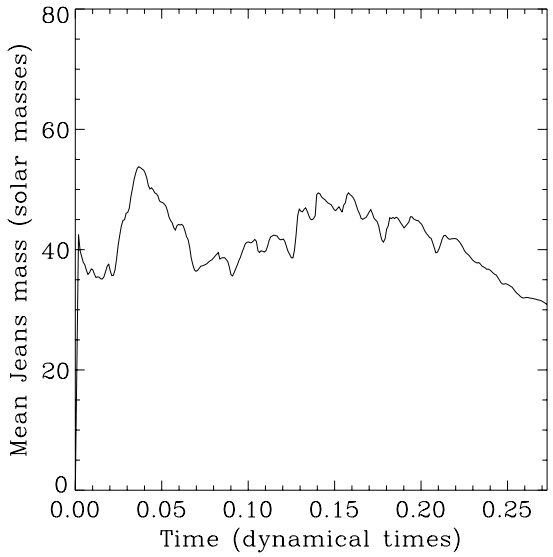

Figure 20. The evolution of the mean Jeans mass in the SL-1 calculation.

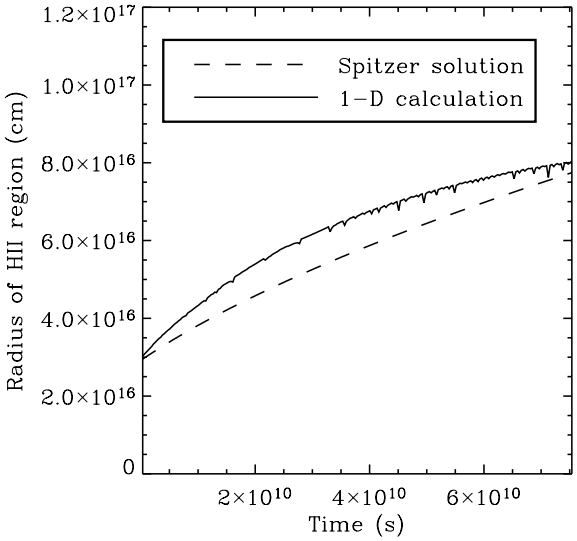

Figure 21. Comparison of the evolution of the H II region under the influence of gravity with the Spitzer solution.

structure in the SL-1 cluster core is complete and compression of material further out in the cluster begins to dominate. The impact of feedback on the star formation process in this system is less clear-cut than in the previous simulations but, in the later stages of the calculation, feedback is again aiding the fragmentation process. Although the Jeans mass is well-resolved in this calculation, we did not observe the formation of any new stars. This is due to the fact that a Jeans mass of $\sim 40\,\mathrm{M}_{\odot}$ represents a significant fraction of the total residual gas content of the cluster and it is very difficult to gather such a large quantity of material into one place.

The competition between the constructive and destructive impacts of feedback seen in these simulations is also apparent in the behaviour of systems such as M16 and NGC 3603 in which the effects of massive stars on molecular clouds can be observed directly. Based on their observations of NGC 3603, Tapia et al. (2001) conclude that, while the cluster HD 97950 is evidently destroying its natal molecular cloud, the existence of embedded infrared objects near the ionization fronts also implies that triggered star formation is in progress in NGC 3603. Hester et al. (1996) observe that the erosion of the famous gas pillars in the Eagle nebula is 'fixing' the masses of the stars already formed by preventing them from accreting additional material, just as occurred in our SL-1 calculation. However, they also suggest that radiatively driven implosion may be responsible for stimulating the formation of the young stars in M16. However, McCaughrean & Andersen (2002) show that only $\sim$15 per cent of the gaseous clumps in M16 [dubbed evaporating gaseous globules (EGGs) by Hester et al. (1996)] contain infrared point sources indicative of young stars or protostellar objects. It is evident that the problem of induced star formation is a difficult one requiring much further study.

5 IMPACT OF GRAVITY AND CLOUD STRUCTURE ON THE EFFECTIVENESS OF FEEDBACK

The initial conditions of the calculations presented above are clearly very complex. It is obviously of interest to attempt to determine what influence the structure present in our model protoclusters had on their evolution. It was already remarked that the radial density profiles of the models resemble power laws. Smoothing out over 4π sr the mass in spherical shells centred on $r = 0$ revealed that all the model clusters could be well represented by density profiles of the form

$$\rho = \begin{cases} \rho_{\mathrm{core}} & \text{for} \quad r \leqslant r_{\mathrm{core}} \\ \rho_{\mathrm{core}}(r_{\mathrm{core}}/r)^{-2} & \text{for} \quad r_{\mathrm{cluster}} > r > r_{\mathrm{core}}, \end{cases} \tag{2}$$

where $r_{\mathrm{core}} \simeq 0.01 r_{\mathrm{cluster}}$.

We used a simple one-dimensional Lagrangian code to investigate the effect of the structures of the clouds on their evolution. The input physics of the code consisted of fluid dynamics, gravity and photoionization (note that the self-gravity of the gas was included in the calculation of gravitational forces to give better consistency with our SPH simulations). This code was used to model the evolution of initially static density profiles with the form of equation (2) corresponding to the high- and low-density SPH calculations.

There are four important length-scales inherent in this problem. The initial efficacy of photoionization is determined by the *initial* Strömgren radius, R_{s} corresponding to the gas number densities in the cores of the smoothed clouds. The *maximum* efficacy of photoionization is determined by the equilibrium Strömgren radius, R_{eq} at which the H II region would come into pressure equilibrium with the ambient gas if the ambient gas were of density ρ_{core} everywhere. In the absence of gravity, the subsequent evolution of the H II region would be determined purely by the size of R_{s} or R_{eq} relative to the third length-scale of interest, the cloud core radius, r_{core}. The propagation of an ionization front resulting from the sudden ignition of an ionizing source in an initially stationary uniform medium passes through two phases (see e.g. Spitzer 1978). In the very early stages of the development of the H II region, the recombination rate inside the H II region is small compared with the photon output of the source and most of the photons emitted ionize fresh material at the ionization front. The propagation speed of the front is highly supersonic and the time-scale on which the H II region grows is much shorter than any relevant dynamical time-scales. The gas remains everywhere approximately motionless in this evolutionary phase, during which the ionization front is termed an 'R-type' front. As the H II region grows, the radiation reaching the ionization front becomes geometrically diluted and the recombination rate inside the H II region increases, eventually becoming comparable to the

Downloaded from https://academic.oup.com/mnras/article/358/1/291/1036608 by U.S. Department of Justice user on 16 August 2022

Table 2. Comparison of the important length-scales in the high- and low-density calculations.

Run	R_s (cm)	R_{eq} (cm)	R_{esc} (cm)	r_{core} (cm)
UH-1	2.0×10^{15}	3.4×10^{17}	5×10^{16}	3.8×10^{16}
SL-1	3.0×10^{16}	5.1×10^{18}	4×10^{15}	8.2×10^{16}

photon luminosity of the source. The propagation speed of the ionization front therefore decreases continually. When the speed of the ionization front becomes comparable to the speed of sound in the H II region, the time-scale on which fresh gas is ionized becomes longer than the sound-crossing time of the system and the H II region expands dynamically, driving a strong shock before it. The ionization front is subsequently known as a 'D-type' front and is confined behind the shock front because, in a uniform medium, the shock is always able to sweep up enough material to confine the ionization front. If the medium in which the ionizing source is born is not uniform, but instead possesses a power-law density profile $\rho \sim \rho_{core}^{-w}$, this is not necessarily true. It can be shown that, in cored density profiles in which the density of the envelope falls off more steeply than $w = \frac{3}{2}$, if the H II region is able to expand beyond the core during either the initial R-type phase or the D-type phase, it will expand to infinite radius (Franco et al. 1990).

Most of the theoretical work on H II regions completed to date assumes the gas involved to be initially at rest and neglects the effects of the gravitational field of the radiation source. The addition of gravitational forces introduces a fourth length-scale to the problem, which we term the gravitational escape radius, R_{esc}. This is the radius within which the escape velocity due to the gravitational field of the ionizing source and of the gas itself exceeds the thermal velocity of the ionized gas. One might expect that an H II region which achieves ionization equilibrium within this radius will not be able to expand.

We list in Table 2 the four length-scales described above corresponding to the smoothed versions of the high- and low-density SPH calculations. In both cases, the initial Strömgren radii of the clouds are inside their core radii, so the H II regions in both calculations are expected to come into ionization equilibrium and enter their D-type expansion phase before encountering the power-law slope in the density profiles. Also in both cases, the equilibrium Strömgren radii lie outside the core radii. In the absence of gravity, one would therefore expect the H II regions in both calculations to expand beyond the cores and to ionize the whole clouds. However, the clouds differ in that, in the high-density case, the initial Strömgren radius lies *inside* the gravitational escape radius, whereas in the low-density cloud, the reverse is true. This suggests that the H II region in the high-density cloud may be prevented from expanding, but that in the low-density cloud, the H II region should be able to overflow the core and to then engulf the whole cloud.

Both predictions are borne out by the results from our one-dimension calculations. In the high-density case, the H II region had almost no effect on the dynamics of the gas, which rapidly settled into a steady free-fall accretion flow. In the low-density calculation, the expansion of the ionization front is similar to the well-known Spitzer solution which would obtain in the absence of gravity in the uniform-density core of the cloud, given by

$$R(t) = R_s \left(1 + \frac{7}{4}\frac{c_s t}{R_s}\right)^{4/7}, \quad (3)$$

where c_s is the isothermal speed of sound in the ionized gas.

As shown in Fig. 21, the H II region in our calculation expands faster than the Spitzer solution as it accelerates down the density gradient generated by the accretion flow and rapidly reaches the core radius. Once it leaves the core, the H II region will expand rapidly to engulf the whole cloud.

We therefore find that gravity prevents the H II region expanding in the case where the Strömgren radius is well inside the escape radius, but indirectly accelerates the expansion for $R_s > R_{esc}$ by creating a density gradient.

The results of our one-dimensional calculations suggest that, if the UH-1 and SH-1 protoclusters investigated in Section 3 had not possessed a high degree of structure, the effect on them of the photoionizing radiation from their central massive stars would have been negligible. However, it appears that the structure present in the SL-1 calculation lessened the effectiveness of feedback by preventing the source from ionizing all the gas in the system, as the one-dimensional calculation suggests that it should. As one might expect, the 'clumpiness' of the gas makes the impact of photoionization less dependent on the mean gas density.

These results have interesting implications for the problem of the energy source required to ionize the diffuse interstellar gas (DIG) in spiral galaxies. The DIG exists as a layer of ionized hydrogen filling large volume fractions of spiral galaxies and accounting for up to 50 per cent of their Hα flux (Ferguson et al. 1996). The Lyman continuum power required to ionize the DIG is too large to be accounted for by winds or supernovae and the only remaining plausible source is the photoionizing radiation from OB stars. In order to produce diffuse ionized gas, this radiation must be able to escape from H II regions. Our results show that this is indeed possible but that the quantity of radiation that can escape an H II region depends strongly on its internal structure. In our high-density simulations, the fractions of flux escaping the clouds towards the ends of the runs was ~20 per cent ($\sim 1.2 \times 10^{49}$ s^{-1}), whereas the H II region in the corresponding one-dimensional calculation was trapped within the cluster. It was therefore only due to the clumpiness of the gas that any radiation was able to escape the H II region. Conversely, in the low-density SPH simulations, ~70 per cent ($\sim 1.4 \times 10^{49}$ s^{-1}) of the flux was escaping by the end of the run. In the one-dimensional calculation, the cloud became fully ionized and the fraction of flux escaping would approach unity. The inhomogeneities in the gas therefore limited the escaping flux in the low-density calculations. Although the fluxes should be treated only as estimates, as the boundaries of our clouds were arbitrary, our results suggest that large fluxes of ionizing photons can escape from H II regions and are thus a potential means of ionizing the DIG. Reynolds in Lesch et al. (1997) calculates that ~15–20 per cent of the total Lyman continuum from O-stars would be sufficient to ionize the DIG in the Galaxy, which our results demonstrate is feasible.

Our calculations also provide an interesting insight into the ultracompact H II region lifetime problem (Wood & Churchwell 1989). Several authors (e.g. de Pree et al. 1995; Garcia-Segura & Franco 1996) have suggested that the expansion of ultracompact H II regions may be prevented by pressure confinement if the temperatures and number densities of the cores in which the H II regions form are significantly higher than those typically assumed for molecular clouds or if additional magnetic or turbulent pressures are present. The expansion of the H II regions in our SPH calculations is indeed strongly affected by dynamical pressure, namely the ram-pressure of the accretion flows delivering gas into the vicinity of the radiation source. However, because these ram-pressures are highly anisotropic, they only hinder or prevent expansion of the H II region in some directions, leading to the complex geometry shown in Fig. 7. Our one-dimensional calculations also suggest that the gravitational field of the source may be able to prevent H II region expansion.

Downloaded from https://academic.oup.com/mnras/article/358/1/291/1036608 by U.S. Department of Justice user on 16 August 2022

Koo et al. (1996) and Kurtz et al. (1999) both conducted surveys of UCHIIRs in which they found evidence for extended emission around many sources which are regarded as compact. If it can be shown that such extended emission is directly related to the compact sources, this may alleviate the lifetime problem as it implies that the H II regions *have* expanded as expected. However, the source of the clumps of high-density ionized gas embedded within extended, lower-density H II remains a problem. This topic is discussed by Franco et al. (2000), who suggest that the clumps may be formed by instabilities during the formation or expansion phase of the H II region. We suggest another possibility. The densest ionized gas in our simulations is located at the tips of the filamentary accretion flows and is visible in Fig. 7 as the small white region at the centre of the image. Although this very dense material is constantly being accreted, it is also constantly being replenished by the accretion flows, so the small region of very dense ionized gas near the source will persist for as long as the accretion flows.

The interaction of H II regions with accretion flows in the presence of gravitational fields is evidently a problem which requires a great deal of further study.

6 CONCLUSIONS

We have undertaken the first ever hydrodynamic simulations of star cluster formation that incorporate feedback from ionizing radiation from massive stars. These simulations differ from preceding feedback simulations (e.g. Tenorio-Tagle et al. 1986) in that the initial gas density distribution has the highly complex morphology that one would expect to develop in the gravitationally unstable regions of molecular clouds. In particular, the ionizing source is located in the cluster core, close to the intersection of a number of dense, nearly radial filaments of inflowing gas. Our chief results are as follows.

(i) Radial filaments of gas in the cluster core provide a mechanism for collimating a number of outflows from the vicinity of the massive star. The opening angles, flow velocities and mass-loss rates compare very favourably with those of observed outflows in regions of massive star formation. A more detailed analysis is required in order to assess what fraction of outflows can be collimated by the gaseous environment in this way, compared with the number of sources that require an intrinsic collimation mechanism close to the star.

(ii) The simulations demonstrate both positive and negative feedback effects. Ionization reduces the rate of inflow of gas into the cluster core and thus reduces the growth rate of the most massive star compared with control simulations without feedback. On the other hand, feedback also enhances the production of *new* stars due to lateral compression of neutral gas in the walls separating adjacent ionized flows. The latter process is not fully resolved by our calculation, so we cannot at present quantify the relative importance of positive and negative feedback effects.

(iii) We find that ionization exacerbates small asymmetries in the initial gas distribution and rapidly generates grossly asymmetric gas structures (see Figs 4, 10 and 16). The impact of ionization on the cloud (in terms of the volume-filling factor of ionized gas) can be greatly enhanced by the anisotropic gas distribution. The 'damage' inflicted by ionization can readily be assessed from Fig. 10. In contrast, if the same ionizing source is ignited in a cluster where the gas distribution was an azimuthally averaged rendition of the gas distribution we employ here, we find that the ionizing region would be completely trapped within the cluster core (i.e. within $\sim$0.02 pc of the source). However, we also find that the impact of feedback can be decreased by such structure, as shown by comparing our SL-1 run with the corresponding azimuthally averaged calculation, the latter suggesting that all the gas in the system should be ionized. Instead, the formation of high-density structures protects some of the gas in the system, at least temporarily, from the radiation field, allowing it to remain neutral.

(iv) We find that although the gas in our simulations absorbs a quantity of thermal and kinetic energy from the ionizing source that comfortably exceeds the gravitational binding energy of the cluster, this *is not* a good criterion for assessing whether the cluster will ultimately remain bound or not. The reason for this is simply that most of the energy is acquired by a relatively small fraction of the gas (i.e. that involved in the outflows) which is accelerated to a speed that significantly exceeds the cluster escape velocity and carries the energy out of the system.

(v) Because of the clumpy nature of the gas in our simulations, we found that significant fractions of the ionizing fluxes of our sources were able to escape our H II regions entirely, although whether or not the fraction escaping is enhanced or decreased by the structure of the gas depends on the mean gas density. Our results demonstrate that radiation leaking from H II regions is a plausible means of ionizing the diffuse ionized gas in spiral galaxies.

The above results suggest that the issue of unbinding clusters by photoionization, and of the local star formation efficiency in massive star-forming regions needs to be revisited. The fact that massive stars, in simulations and in reality, form in the cluster core where the gas is densest, in general, inhibits photoionization feedback, although this effect may be mitigated by stellar wind clearing, which is not included in these simulations. As one would expect, density is the key parameter that controls the efficiency of feedback (contrast Fig. 10 with Fig. 16). This suggests that there are certain areas of mass-radius parameter space for the progenitor clouds of the protoclusters that allow the runaway growth of massive stars in the cluster core. Thus, quite apart from the issue of whether massive stars form by coalescence or by accretion, the density dependence of feedback provides an additional reason why the most massive stars form in the densest cluster environments.

ACKNOWLEDGMENTS

We gratefully acknowledge the anonymous referee for very helpful comments. JED acknowledges support from a PPARC studentship. CJC gratefully acknowledges support from the Leverhulme Trust in the form of a Phillip Leverhulme prize. The computations reported in Section 3.1 were performed using the UK Astrophysical Fluids Facility.

REFERENCES

Adams F. C., 2000, ApJ, 542, 964
Arthur S. J., Kurtz S. E., Franco J., Albarrán M. Y., 2004, ApJ, 608, 282
Battinelli P., Capuzzo-Dolcetta R., 1991, in ASP Conf. Ser. Vol. 13, The Formation and Evolution of Star Clusters. Astron. Soc. Pac., San Francisco, p. 139
Beuther H., Schilke P., Geuth F., McCaughrean M., Anderson M., Sridharan T. K., Menten K. M., 2002, A&A, 387, 931
Boily C. M., Kroupa P., 2003, MNRAS, 338, 673
Bonnell I. A., Bate M. R., 2002, MNRAS, 336, 659
Bonnell I. A., Bate M. R., Zinnecker H., 1998, MNRAS, 298, 93
Churchwell E., 1997, ApJ, 479, L59
Clarke C., Oey M. S., 2002, MNRAS, 337, 1299

Downloaded from https://academic.oup.com/mnras/article/358/1/291/1036608 by U.S. Department of Justice user on 16 August 2022

Clarke C. J., Bonnell I. A., Hillenbrand L. A., 2000, Protostars and Planets IV. Univ. Arizona Press, Tucson, p. 151
Davis C. J., Varricatt W. P., Todd S. P., Ramsay Howat S. K., 2004, A&A, 425, 981
Dekel A., Silk J., 1986, ApJ, 303, 39
de Pree C. G., Rodriguez L. F., Goss W. M., 1995, Rev. Mex. Astron. Astrofis., 31, 39
Diaz-Miller R. I., Franco J., Shore S. N., 1998, ApJ, 501, 192
Edgar R., Clarke C., 2003, MNRAS, 338, 962
Edgar R., Clarke C., 2004, MNRAS, 349, 678
Elmegreen B. G., 1998, in ASP Conf. Ser. Vol. 148, Origins. Astron. Soc. Pac., San Francisco, p. 150
Elmegreen B. G., 2000, ApJ, 530, 277
Elmegreen B. G., Palouš J., Ehlerová S., 2002, MNRAS, 334, 693
Ferguson A. M. N., Wyse R. F. G., Gallagher J. S., Hunter D. A., 1996, AJ, 111, 2265
Franco J., Garcia-Segura G., 1996, Bull. Am. Astron. Soc., 28, 848
Franco J., Tenorio-Tagle G., Bodenheimer P., 1990, ApJ, 349, 126
Franco J., Kurtz S. E., Garcia-Segura G., Hofner P., 2000, Ap&SS, 272, 169
Garcia-Segura G., Franco J., 1996, ApJ, 469, 171
Geyer M. P., Burkert A., 2001, MNRAS, 323, 988
Goodwin S. P., 1997, MNRAS, 284, 785
Hartmann L., 2003, ApJ, 585, 398
Hegmann M., Kegel W. H., 2003, MNRAS, 342, 453
Hester J. J. et al., 1996, AJ, 111, 2349
Hills J. G., 1980, ApJ, 235, 986
Hobson M. P., Padman R., 1993, MNRAS, 264, 161
Hobson M. P., Scheuer P. A. G., 1993, MNRAS, 264, 145
Kessel-Deynet O., Burkert A., 2000, MNRAS, 315, 713
Klein R. I., Fisher R. T., Krumholz M. R., McKee C. F., 2003, in Arthur J., Henney W., eds, Rev. Mex. Astron. Astrofis. Conf. Ser., Vol. 15, Winds, Bubbles and Explosions: A Conference to Honor John Dyson. UNAM, Mexico, p. 92
Koo B., Kim K., Lee H., Yun M., Ho P. T. P., 1996, ApJ, 456, 662
Kumar M. S. N., Bachiller R., Davis C. J., 2002, ApJ, 576, 313
Kurtz S. E., Watson A. M., Hofner P., Otte B., 1999, ApJ, 514, 232
Lada C. J., Margulis M., Dearborn D., 1984, ApJ, 285, 141
Lesch H., Dettmar R., Mebold U., Schlickeiser R., eds, 1997, The Physics of Galactic Halos. John Wiley & Sons, New York
McCaughrean M. J., Andersen M., 2002, A&A, 389, 513
McKee C. F., 1989, ApJ, 345, 782
McKee C. F., Ostriker J. P., 1977, ApJ, 218, 148
Martins F., Schaerer D., Hillier D. J., Heydari-Malayeri M., 2004, A&A, 420, 1087
Röllig M., Hegmann M., Kegel W. H., 2002, A&A, 392, 1081
Shaviv N. J., 2001, MNRAS, 326, 126
Shepherd D. S., Churchwell E., Wilner D. J., 1997, ApJ, 482, 355
Spitzer L., 1978, Physical Processes in the Interstellar Medium. Wiley-Interscience, New York, p. 333
Tapia M., Bohigas J., Pérez B., Roth M., Ruiz M. T., 2001, Rev. Mex. Astron. Astrofis., 37, 39
Tassis K., Abel T., Bryan G. L., Norman M. L., 2003, ApJ, 587, 13
Tenorio-Tagle G., Bodenheimer P., Lin D. N. C., Noriega-Crespo A., 1986, MNRAS, 221, 635
Tenorio-Tagle G., Silich S. A., Kunth D., Terlevich E., Terlevich R., 1999, MNRAS, 309, 332
Tenorio-Tagle G., Palouš J., Silich S., Medina-Tanco G. A., Muñoz-Tuñón C., 2003, A&A, 411, 397
Whitworth A., 1979, MNRAS, 186, 59
Whitworth A. P., Francis N., 2002, MNRAS, 329, 641
Witt A. N., Gordon K. D., 1996, ApJ, 463, 681
Wolfire M. G., Cassinelli J. P., 1986, ApJ, 310, 207
Wolfire M. G., Cassinelli J. P., 1987, ApJ, 319, 850
Wood D. O. S., Churchwell E., 1989, ApJS, 69, 831
Yorke H. W., Sonnhalter C., 2002, ApJ, 569, 846
Yorke H. W., Tenorio-Tagle G., Bodenheimer P., Rozyczka M., 1989, A&A, 216, 207
Zuckerman B., Evans N. J., 1974, ApJ, 192, L149

This paper has been typeset from a TEX/LATEX file prepared by the author.

Downloaded from https://academic.oup.com/mnras/article/358/1/291/1036608 by U.S. Department of Justice user on 16 August 2022